Spin ordering and dynamics in the frustrated antiferromagnet $YBaCo_4O_{7.1}$

S. Yuan,[1] X. Hu,[1] P. L. Kuhns,[1] A. P. Reyes,[1] J. S. Brooks,[1] T. Besara,[1] T. Siegrist,[1,2] H. Zheng,[3] J. F. Mitchell,[3] and M. J. R. Hoch[1,*]

[1]*National High Magnetic Field Laboratory, Florida State University, Tallahassee, Florida 32310, USA*

[2]*Department of Chemical and Biochemical Engineering, FAMU/FSU College of Engineering, Tallahassee, Florida 32310, USA*

[3]*Materials Science Division, Argonne National Laboratory, Argonne, Illinois 60439, USA*

(Received 4 October 2013; revised manuscript received 30 January 2014; published 19 March 2014)

The stoichiometric 114-layered material $YBaCo_4O_7$ exhibits long-range antiferromagnetic order below a Néel temperature of 106 K. Nonstoichiometric $YBaCo_4O_{7.1}$, which contains a relatively small amount (1.4%) of interstitial oxygen, has recently been shown to have drastically modified magnetic properties compared to the parent compound. The present experiments have used magnetization, ac susceptibility, and zero applied field NMR to study the spin configuration and spin dynamics in a single crystal of $YBaCo_4O_{7.1}$ as a function of temperature below 100 K. Evidence has been obtained for a magnetic transition at 80 K corresponding to some form of spin freeze-out. Based on previous results for the stoichiometric material, it is likely that the freezing process involves spins in the triangular layers in this frustrated antiferromagnet. At lower temperatures, dynamic effects persist and below 50 K a fraction of the spins, located primarily in the kagome layers, constitute what may be termed a viscous spin liquid component. For $T < 10$ K, a disordered or glasslike spin structure, with a large distribution of spin correlation times, emerges as the low-temperature state of the spin system.

DOI: 10.1103/PhysRevB.89.094416 PACS number(s): 75.25.−j, 75.50.Lk, 76.60.Jx

I. INTRODUCTION

The cobalt oxide $YBaCo_4O_7$ is a frustrated antiferromagnet (AF) with a unique magnetization topology that can be considered as a variant of the pyrochlore structure. The crystal structure is made up of stacked 2D layers of Co ions arranged in alternating triangle (T) and kagome (K) planes with the T planes stacking in an ...AAA... sequence, while the pyrochlore has an ...ABC... sequence. This leads to a structural motif consisting of trigonal bipyramids of magnetic ions rather than the tetrahedral coordination found in pyrochlores. Geometric frustration, inherent to the structure, leads to unconventional spin configurations which give rise to unusual magnetic properties below 100 K [1–5]. The layered structure of the material facilitates the uptake of additional interstitial oxygen atoms to form nonstoichiometric (NS) $YBaCo_4O_{7+\delta}$ with $0 < \delta \leq 1.6$. The powder form of this material has potential for oxygen storage applications since the uptake process is reversible with oxygen being released when the temperature is raised above 400 °C [6–9]. Incorporation of additional oxygen into the $YBaCo_4O_7$ lattice induces δ-dependent changes in the crystal structure. Specifically, changes occur in the coordination geometry and in the bond lengths of the oxygen polyhedra that surround the Co ions. Magnetization measurements show that the structural changes alter the low-temperature magnetic properties compared to those of the stoichiometric (S) material [10–12]. In particular, all evidence of long-range order is lost as the oxygen stoichiometry is increased from $\delta = 0$ to 0.1, indicating the fragility of the ordered state [13]. Details of the spin structure in $YBaCo_4O_{7.1}$ remain to be determined. Neutron diffraction experiments reveal diffuse scattering at low temperatures and this suggests that the ground state of $YBaCo_4O_{7+\delta}$ involves spin disorder for the range $0.1 < \delta \leq 1.0$ [10,13]. Figure 1, based on information given in Ref. [10], compares the T and K layer structures of the S material $YBaCo_4O_7$ with that of the NS material $YBaCo_4O_8$ ($\delta = 1.0$). The crystal used in the present experiments has $\delta = 0.1$ with interstitial oxygen content that lies between the two extremes shown in Fig. 1. Co ions are located in the shaded oxygen tetrahedral, which are represented by their basal planes. Some tetrahedra are converted to octahedra by the excess oxygen as indicated in the figure.

The parent S material $YBaCo_4O_7$ undergoes a symmetry-lowering transition from a trigonal phase to an orthorhombic phase at 310 K but no such transition is found in the low δ material $YBaCo_4O_{7.1}$, which retains the trigonal $P31c$ structure over a wide temperature range [14]. In $YBaCo_4O_7$ the symmetry-lowering transition relieves geometric frustration and allows the triangle spins to order antiferromagnetically in the ab plane below the Néel temperature $T_N = 106$ K. For $T < T_N$, the spins in $YBaCo_4O_7$ are ordered in ferromagnetic (FM) chains along the c axis. Evidence for short-range FM correlations persisting along c for $T > T_N$ is provided by diffuse neutron scattering [2]. It is clearly of interest to examine the low-temperature spin configuration in the NS material and to compare this with the available information for the S case. A question of interest is the following: do short-range spin correlations of the type found above T_N in the S material occur in the NS system, which does not exhibit long-range order down to liquid helium temperatures? Alternatively, can the NS system be used to gain understanding of the short-range order in a putative defect-free system for which the structural phase transition has been suppressed? Our magnetization, ac susceptibility and zero applied field (ZF) NMR experiments reveal that some form of spin ordering occurs at a transition temperature of 80 K but that this ordering is qualitatively different from that in the S material. Below 80 K in the NS system, dynamic effects persist for a significant fraction of the spins down to less than 10 K. The findings are consistent with sequential freeze-out processes occurring with decreasing temperature first in the T layers and then at lower temperatures in the K layers.

*Corresponding author: hoch@magnet.fsu.edu

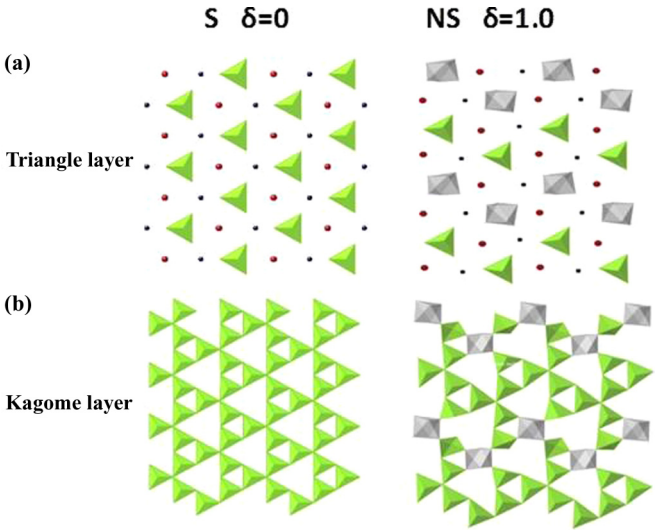

FIG. 1. (Color online) Representation of the triangle (a) and kagome (b) layer structures in $YBaCo_4O_{7+\delta}$ showing the stoichiometric (S) case with $\delta = 0$ on the left and a nonstoichiometric (NS) case with $\delta = 1.0$ on the right. The shaded regions (green in color) represent oxygen tetrahedra that surround Co ions. Some conversion of oxygen tetrahedra into octahedra, represented by the shaded octahedra (gray), is produced by excess interstitial oxygen as shown for the $\delta = 1$ NS material. The layer structure in the $\delta = 0.1$ NS crystal used in the present experiments is expected to exhibit some structural features similar to those found in the $\delta = 1.0$ case. The figure is based on information and results given in Ref. [10].

II. EXPERIMENTAL DETAILS

The $YBaCo_4O_{7.1}$ single crystal used in the experiments was prepared by controlled high temperature oxidation of an S single crystal that was grown in a float-zone furnace. Oxygen content was verified post-treatment by thermogravimetric analysis of a ground crystal sample. The orientations of the crystal axes in the cylindrical sample (diameter 4 mm, length 5 mm) were determined by single crystal x-ray diffraction using a four-axis Enral Nonius CAD-4 diffractometer. Magnetization measurements were made as a function of temperature using a Quantum Design superconducting quantum interference device (SQUID) magnetometer in an applied field of $\mu_0 H = 0.1$ T. The temperature dependence of the ac susceptibility was determined with a Quantum Design physical property measurement system (PPMS) using an ac field of 7.5 Oe in zero dc applied field. The present NMR work has focused on ^{59}Co measurements in ZF making use of the large hyperfine fields in this material. An attempt was made to detect ^{89}Y NMR signals in a variable applied field but this was not successful, even at the lowest temperatures used, presumably because of the very short relaxation times for this nucleus. The ^{59}Co NMR spectra and relaxation rates were obtained with a computer-controlled variable frequency spin-echo spectrometer. The RF field was directed either parallel to c or at various orientations with respect to the [110] direction in the ab plane. Details of the ZF NMR approach to the determination of AF spin configurations are given in Ref. [15].

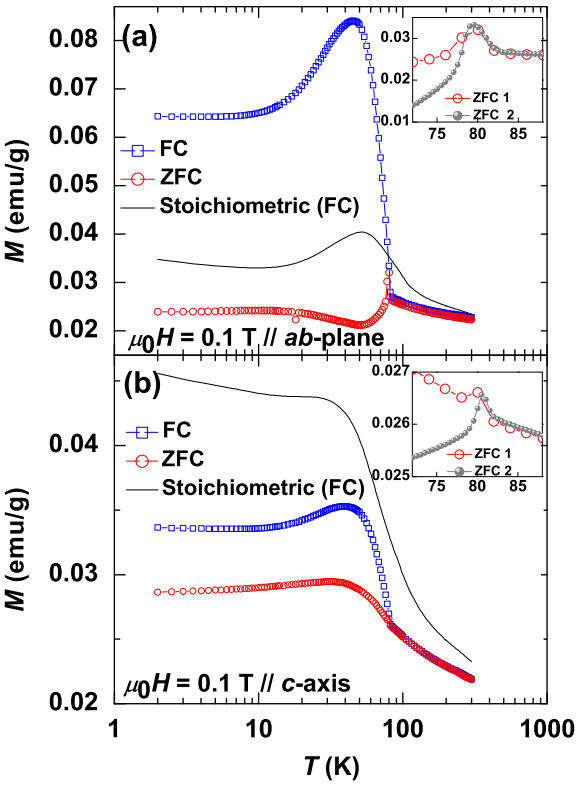

FIG. 2. (Color online) Magnetization (M) curves for a NS $YBaCo_4O_{7.1}$ single crystal as a function of temperature following zero-field-cooling (ZFC) and field-cooling (FC) for $H = 0.1$ T (a) in the ab plane and (b) parallel to the c axis. The solid curve shows the behavior of stoichiometric $YBaCo_4O_7$ (Ref. [15]). The FC and ZFC M plots for the NS crystal show a change in slope at 80 K with thermal history dependent properties below 80 K, as shown in the insets in Figs. 2(a) and 2(b) for different warming procedures following cool down to 2 K. In the first procedure (ZFC 1, open circles) the sample was gradually heated to 90 K, at 1 K/min, while in the second procedure (ZFC 2, closed circles) the sample was first heated to 70 K, at 5 K/min, before scanning the transition region 70–90 K at 1 K/min. Both insets show a cusplike feature in M close to 80 K.

III. EXPERIMENTAL RESULTS

A. Magnetic properties

Figure 2 shows the magnetization M for $YBaCo_4O_{7.1}$ as a function of temperature in an applied field $\mu_0 H = 0.1$ T directed firstly, in Fig. 2(a), in the ab plane and secondly, in Fig. 2(b), parallel to the crystal c axis. Both field-cooled (FC) and zero-field-cooled (ZFC) initial conditions were used with M measured in warming runs. FC magnetization plots for the S crystal, with the same orientations of H with respect to the crystal axes [15], are shown, for comparison, as the full curves in Figs. 2(a) and 2(b). For H along c, the FC NS response is fairly similar to that of the FC S crystal, but is reduced in magnitude and exhibits a maximum at 40 K, whereas the S crystal magnetization continues to increase as the temperature is lowered. For H in the ab plane the FC NS magnetization is roughly double that of the S crystal. Both the FC and ZFC magnetization curves for the NS crystal show an

abrupt change in slope at 80 K with thermal history-dependent magnetic properties below 80 K, as given in the insets in Figs. 2(a) and 2(b). The data in the insets correspond to two different warming procedures following ZF cooling to 2 K. In the first procedure (open circles), designated ZFC 1, the sample was gradually warmed at 1 K/min from 2 to 90 K, while in the second procedure (closed circles), ZFC 2, the sample was fairly rapidly heated to 70 K at 5 K/min before scanning the transition region more slowly from 70–90 K at 1 K/min. The magnetization curves clearly depend on the procedure used, most dramatically for H parallel to the c axis. The observed trends in M with T in the range $50 < T < 80$ K undergo a change below $T \sim 50$ K with M becoming temperature independent for $T < 10$ K. The difference between the ZFC and FC magnetization curves implies spin-glass-like properties at low temperatures.

The anisotropy in the M versus T curves in Figs. 2(a) and 2(b), measured in an applied field of 0.1 T, suggests that the spins in the $\delta = 0.1$ NS sample are not isotropically distributed in small applied fields. However, no orientation dependence of the FC magnetization in the ab plane was found in experiments in which the crystal was rotated about the c axis. Neutron scattering experiments indicate that considerable spin-disorder persists at low temperatures [13].

The cusp feature in M versus T found at 80 K for the NS sample and, which is most distinct for H in the ab plane, shows that some form of magnetic order, not necessarily long-range order, is established below 80 K. Figure 3 shows the ac susceptibility, over the frequency range 1 Hz–1 kHz, as a function of temperature in warming runs following cooling to 70 K. Frequency *independent* peaks in both the real part χ' [Fig. 3(a)] and the imaginary part χ'' [Fig. 3(b)] are found at 81 K. This finding suggests that while $YBaCo_4O_{7.1}$ exhibits history-dependent magnetic behavior at temperatures below 80 K, the transition is not a conventional spin glass transition. Measurements of the ac susceptibility for $T \ll 80$ K show no marked features with increasing temperature in the range 10 to 20 K, with poor signal-to-noise ratio.

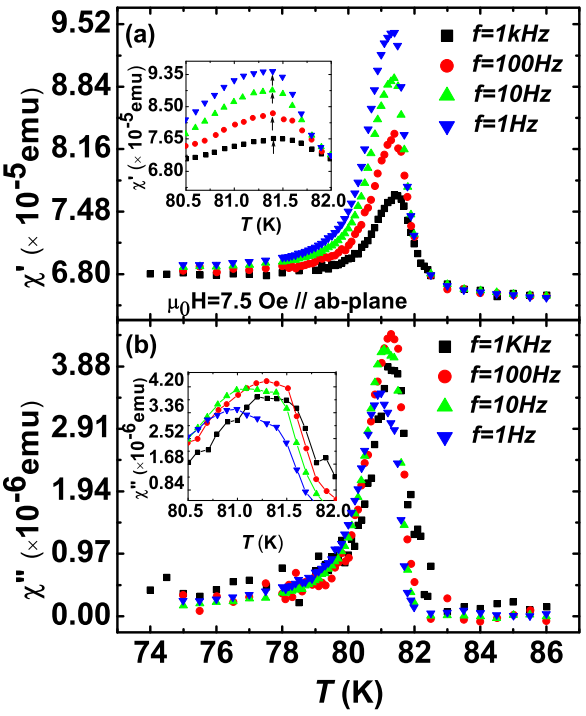

FIG. 3. (Color online) Real (χ') (a) and imaginary (χ'') (b) components of the ac susceptibility of the $YBaCo_4O_{7.1}$ single crystal as a function of temperature and frequency in the range 1–1000 Hz with an ac field of 7.5 Oe and zero dc field. The peak at ~81 K corresponds to the cusp in the magnetization results shown in Fig. 2. The insets show an expanded T scale.

B. Zero applied field NMR

The magnetization behavior described above motivated us to obtain information on the spin configuration in the $\delta = 0.1$ crystal by means of ZF NMR experiments using ^{59}Co ($I = 7/2$, $\gamma/2\pi = 10.03$ MHz/T) as a probe of the local hyperfine (HF) field. This microscopic approach has recently been applied to stoichiometric $YBaCo_4O_7$ and details are given in Ref. [15]. Information on the HF orientations, which are linked to the spin orientations, is obtained by directing the RF field along various directions in the crystal and comparing the NMR spectra that are obtained at each orientation.

Figure 4 shows a comparison of the ^{59}Co ZF spectra at 2 K for a $\delta = 0$ polycrystalline sample and for a $\delta = 0.1$ single crystal with H_1 directed parallel to the c axis. (Use of a polycrystalline sample for the S case ensures that the spectral amplitudes for the T and K spin components are compared properly in this AF ordered material as discussed in Ref. [15].) The amplitudes of the spectra have not been scaled to allow for changes

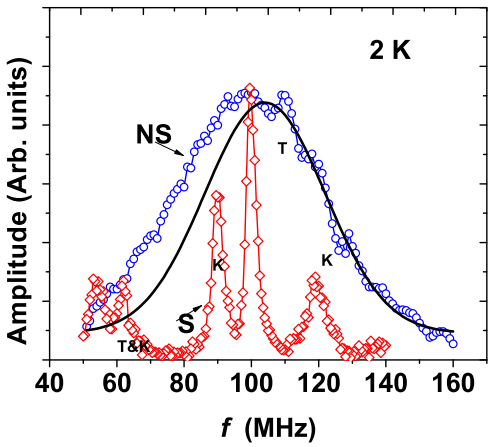

FIG. 4. (Color online) ^{59}Co NMR 2 K spectra obtained in zero applied field for a polycrystalline sample of stoichiometric (S) $YBaCo_4O_7$ (diamonds, red in color) and for a single crystal (with $H_1 \parallel c$, see text) of nonstoichiometric (NS) $YBaCo_4O_{7.1}$ (circles, blue in color). The NS crystal spectrum consists of a broad peak with a maximum at ~104 MHz, while the S material shows distinct peaks at 90, 100, and 120 MHz corresponding to Co^{3+} ions and lower frequency peaks at 55 and 62 MHz, which correspond to Co^{2+} ions as described in Ref. [15]. The labels T and K associate spectral components with triangular layer spins and kagome layer spins, respectively. The solid line, which provides a fit to the high-frequency portion of the NS spectrum ($f > 100$ MHz), is a Gaussian with FWHM of 42 MHz. The origin of the striking difference in spectral shape between the S and NS cases is discussed in the text.

in spectrometer sensitivity with frequency. (The spectrometer response is proportional to f^{α} with $\alpha \sim 2$ so that high frequency components are enhanced compared to low frequency components.) The S crystal gives well resolved ^{59}Co spectral features which permit the T and K spins to be distinguished [15]. The discrete spectral components in the $\delta = 0$ case provide information on the T and K layer HF field configurations, and the associated electron spin configurations, for the Co ions in this mixed valence crystal [15]. The 90, 100, and 120 MHz spectral components are associated with the Co^{3+} ions, while lower frequency components, below 70 MHz, are attributed to the Co^{2+} ions [15]. In contrast, the $\delta = 0.1$ sample gives a broad featureless low-temperature spectrum extending over ~100 MHz with a maximum around 104 MHz. The observed spectrum is consistent with a significant number of the spins in the NS sample being effectively static, on the NMR timescale, with spin correlation times $\tau \gg 10$ μs, and which have a continuous and wide distribution of static HF fields. The 1.7 K spectrum has a full-width half-maximum (FWHM) value of ~50 MHz which corresponds to a HF field distribution of 5 T.

For the NS material $YBaCo_4O_8$ ($\delta = 1$), previous work has shown that the additional oxygen converts a fraction of the oxygen tetrahedra into octahedra as indicated in Fig. 1 [10]. A similar conversion of a fraction of the Co ion tetrahedral sites to octahedral is likely to occur in the $YBaCo_4O_{7.1}$ sample resulting in a reordering of the Co ion t_2 and e states due to the change from T_d to O_h crystal field symmetry. The lack of structural features in the NMR spectra in the NS material prevents separation of contributions from the Co^{2+} and Co^{3+} ions. Based on the spectra for the S crystal it is likely that in the NS case a major contribution to the signals at frequencies above 80 MHz is due to Co^{3+} with Co^{2+} contributing at lower frequencies. This point is discussed in somewhat greater detail below.

Frequency scan ZF ^{59}Co spectra obtained at 1.7 K for four different directions of H_1 in the *ab* plane show no orientation dependence which means that in ZF both the T and K spins have no preferred orientation in the *ab* plane. This finding is consistent with the magnetization measurements made as a function of the applied field orientation in the *ab* plane as described above. The isotropic character of the HF field components in the *ab* plane is consistent with the absence of long-range spin order but does not prove that this is the case. In contrast to the observed magnetization anisotropy, and the dependence of M on the cooling protocol, ZF spectra obtained with H_1 along c following FC in applied fields of 0.1 T and 1.0 T directed in the *ab* plane, showed no change in line shape or, within experimental uncertainty, in amplitude compared to ZFC spectra. As a further check on possible spin anisotropy, NMR spectra at 1.7 K were compared for two orientations of H_1, firstly along the c axis and secondly in the a*b* plane. No discernible difference in spectral shape or amplitude was found provided similar cooling procedures were followed (see below). Using theoretical results, obtained previously [15] for the spectral response of an AF spin system measured as a function of H_1 orientation with respect to the crystal axes, gives the spectrum area ratio, for the two chosen orientations of the $YBaCo_4O_{7.1}$ crystal, as 1.0 if the spins are distributed over 4π and 0.5 if the spins are confined to the *ab* plane. Experimentally, the area of the spectra for H_1 parallel to c and H_1 perpendicular to c agree to within 2%. This analysis

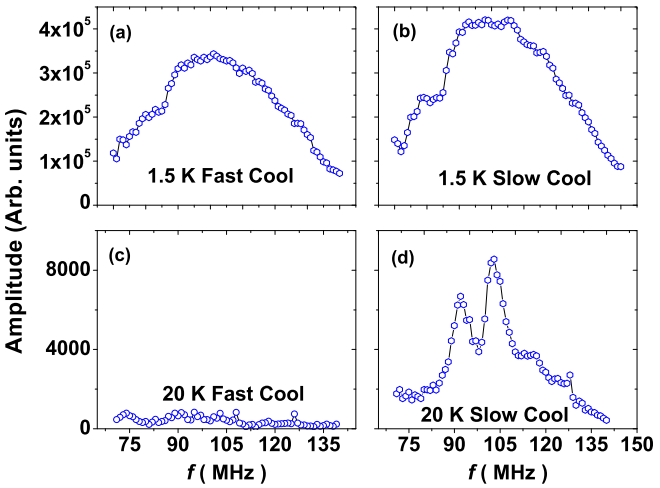

FIG. 5. (Color online) ^{59}Co ZF NMR spectra, with the RF field H_1 parallel to the c axis, for the NS $YBaCo_4O_{7.1}$ crystal following (a) fast cooling (>10 K/min) from 290 to 1.5 K; (b) slow cooling (1 K/min) from 290 to 1.5 K; (c) fast cooling from 290 to 20 K; (d) slow cooling from 290 to 20 K. The spectra obtained at 1.5 K, following the two different cooling procedures, are very similar in shape while the 20 K spectra are quite different with no detectable signal at this temperature in the fast cooling case. The greatly reduced amplitudes are attributed to the operation of Curie's law and to changes in the local spin dynamics with temperature. The slow-cooled NS spectrum in Fig. 5(d) is similar in form to that obtained for the S crystal shown in Fig. 4. An explanation for this finding is given in the text.

permits us to reach the following conclusion: in ZF a major fraction of the K and T spins, which cannot be distinguished in the present NMR experiment, have, to a good approximation, their associated HF fields directed in random orientations over a sphere in what may be descriptively called a *hedgehog* spin configuration. This is in marked contrast to the roughly planar spin configuration found in $YBaCo_4O_7$.

As the temperature is raised, the ^{59}Co ZF-NMR signal-to-noise ratio is found to decrease significantly. Interestingly, the *cooling rate* of the sample is found to determine the signal amplitude and the spectral form for $T > 10$ K. The cooling rate effect on the low-temperature spectra is illustrated in Fig. 5 which shows the spectra obtained at 1.5 and 20 K following fast cooling (>10 K/min) in Figs. 5(a) and 5(c) contrasted with slow cooling (1 K/min) in Figs. 5(b) and 5(d). The spectral shapes at 1.5 K are very similar in both cases, with the slow-cooled spectral amplitude determined at 102 MHz approximately 30% larger than that of the fast-cooled spectrum. It is of interest to note that the amplitude of the fast-cooled 1.5 K spectrum grows towards the amplitude of the slow-cooled spectrum over a period of many hours as shown in Fig. 6. This finding is consistent with gradual freeze-out with time at 1.5 K of spin dynamic effects in some regions of the crystal.

No NMR signal is detected at 20 K following fast cooling from 280 to 20 K, while the slow-cooling protocol, over the same temperature range, results in a spectrum, which is remarkably similar in form to that of the S crystal shown in Fig. 4. It has maximum amplitude approximately 2% of the

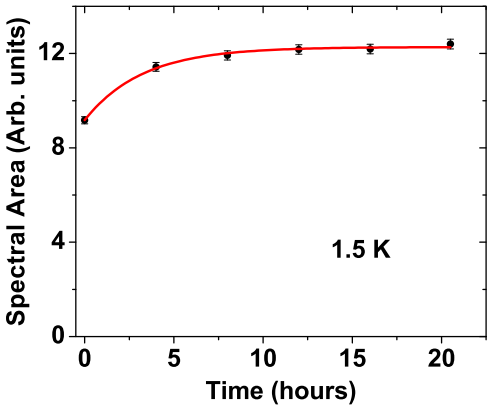

FIG. 6. (Color online) Evolution of the ^{59}Co ZF NMR spectral area with time for the NS $YBaCo_4O_{7.1}$ crystal following fast cooling from 290 to 1.5 K. The fitted curve shows exponential growth with a characteristic growth time of 3.3 hours for the particular conditions used.

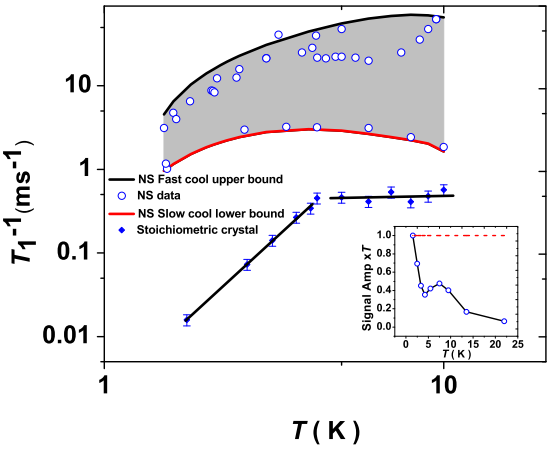

FIG. 7. (Color online) ^{59}Co spin-lattice ($1/T_1$) relaxation rates at 102 MHz as a function of temperature for $YBaCo_4O_7$ (diamonds, blue in color), as presented in Ref. [15], and $YBaCo_4O_{7.1}$ (open circles in shaded band). The straight lines through the $YBaCo_4O_7$ data are guides to the eye. The relaxation rates, obtained from stretched exponential recovery curves, are significantly lower in $YBaCo_4O_7$ than in $YBaCo_4O_{7.1}$, which points to enhanced spin dynamics in the disordered NS material compared to the S case. For the NS crystal, the relaxation rates depend on the cooling procedure with fast cooling (>10 K/min) to $T < 10$ K giving shorter rates than slow cooling (1 K/min) as depicted by the shaded band upper and lower rate limits. The inset shows the spectral amplitude multiplied by T (Curie law correction) as a function of T. The dashed line gives the predicted constant value for a nuclear spin system that follows Curie law behavior. The marked decrease in the scaled NMR signal with T suggests that the number of nuclear spins that contribute to the signal decreases with increasing T as a result of unfreezing of a fraction of the electron moments. The small uptick feature between 4 and 7 K is attributed to a change in the spectral linewidth in this temperature range.

1.5 K spectrum in Fig. 5(b), significantly less than Curie law prediction of 7.5%. The similarity in form of the NS sample spectrum in Fig. 5(d) and that of the S crystal in Fig. 4, suggests that in the slow-cooling experiments on the NS crystal phase separation occurs with the establishment of interstitial oxygen-rich regions and oxygen-poor regions. The oxygen poor regions approximate the pristine S material composition. This finding is briefly discussed in Sec. IV C below.

Figure 7 shows ^{59}Co spin-lattice ZF relaxation rates $1/T_1$ versus T over a limited temperature range for the $\delta = 0.1$ and 0 crystals, obtained at frequencies of 100 MHz, for the S crystal, and 102 MHz for the NS case. The RF field H_1, was directed along the c axis for both sets of measurements. The relaxation rates for the NS sample are considerably higher than those of the S crystal and are found to lie in the shaded band shown in Fig. 7 with values dependent on the cool-down rate. The upper bound of the shaded region corresponds to values obtained in fast-cooling experiments while the lower bound is obtained from slow-cooling experimental results. Intermediate values in the shaded region were obtained in cool-downs in which the rate was not carefully monitored. The NMR recovery curves following a saturation pulse sequence all exhibited stretched exponential form $\exp[(t/T_1)^{\beta}]$ with the stretch parameter $\beta \sim 0.3$ in the NS case and ~ 0.45 in the S case. The nuclear spin-lattice relaxation process in these AF materials involves the electron spin fluctuations as discussed in Ref. [15]. The low β values imply that there is a broad distribution of electron spin correlation times. Correspondingly, there is a distribution of spectral densities in the frequency domain leading to the stretched exponential recovery of the nuclear magnetization which is averaged over all local environments.

The significant increase in the relaxation rates for $\delta = 0.1$compared to $\delta = 0$ points to enhanced spin dynamics in $YBaCo_4O_{7.1}$ compared to $YBaCo_4O_7$. The absence of a transition from trigonal to lower crystal symmetry in the NS system, as a result of the incorporation of a relatively small number of excess oxygen atoms, clearly produces dramatic changes in both the hyperfine field distribution and in the electron spin dynamics in this material. For $\delta = 0.1$, the shortness of the measured spin-spin relaxation time T_2, which approaches 10 μs for $T > 10$ K, prevents reliable relaxation time measurements from being made at temperatures above 10 K. The limited temperature range over which the relaxation rates can be obtained precludes any detailed analysis but is of interest in establishing that spin fluctuations persists at temperatures well below the magnetization cusp temperature $T^* = 80$ K. This finding indicates that for $T \ll 80$ K the dynamic spins are associated with a specific spin subsystem that remains unfrozen. Measurements of the relaxation rates at other frequencies (70 and 125 MHz) give values, and behaviors with T, very similar to those shown in Fig. 7. It follows that fluctuating HF fields, with correlation times on the order of μs, provide the relaxation mechanism and operate across the entire frequency range of the observed spectra.

IV. DISCUSSION

The magnetization and ac susceptibility results together provide strong evidence for the onset of some form of spin ordering at 80 K. However, the nature of the ordering is unclear for this frustrated AF. The evidence for spin glass type disorder is consistent with the absence of long-range order in minority phase isostructural $YbBaCo_4O_{7.2}$ [14]. As mentioned

above, recent neutron scattering results show no long-range order in $YBaCo_4O_{7.1}$ at low temperatures [13]. However, the broad diffuse scattering peaks found below 100 K do provide evidence for short-range magnetic correlations [13]. In order to account for the dramatic differences in magnetic properties of the NS crystal compared to those of the S crystal, we put forward in Sec. IV A below a model for spin ordering and dynamics based on the magnetization and ac susceptibility results described in Sec. III and the previous neutron and NMR findings for the S material [5,15]. The present NMR results are discussed in terms of the proposed model in Secs. IV B and IV C. Section IV D compares the spin properties of the NS and S systems.

A. Proposed model

As a starting point, we assume, based on the available evidence, that the onset of quasi-static AF spin correlations that become important in the NS sample occur at very different temperatures for the K and T spins. Recent neutron scattering experiments on $YBaCo_4O_{7.1}$ confirm the absence of long-range order in the NS material to temperatures as low as 6 K [13]. Based on the findings for the S material, which undergoes an AF ordering transition at 106 K involving the T spins, we suggest that in the NS system the T spins freeze-out at 80 K to form a frustrated AF layered substructure. The cusp in the M versus T plot and the peak in the ac susceptibility are due to this spin freezing transition. The K spins remain dynamic to lower temperatures and form a viscous AF correlated spin substructure for $T < 50$ K, which gradually freezes out to form short-range ordered or spin-glass-like layers below 10 K. The K spins may be more randomly oriented than the T spins and exhibit inhomogeneous behavior within a given layer, with some regions forming dynamically disordered structures, or spin fluid puddles, which have shorter spin correlation times than other regions resulting in a broad correlation time distribution. In putting forward this model we are guided by the findings made for the S material in which AF order in the T layers is established at $T_N = 106$ K, while the K spins exhibit gradual and patchy freeze-out below 50 K [15]. In the NS case, the disordered K layer substructure leads to unusual magnetic properties, as shown in Figs. 2(a) and 2(b) and the insets, which depend markedly on the magnetic history.

B. Low-temperature NMR spectra

The broad featureless ^{59}Co HF-NMR spectrum at 2 K shown in Fig. 4 provides limited information on the spin structure as detailed in Sec. III B. There, it is shown that the lack of dependence of the form of the spectrum on the alignment of the rf field with respect to the crystal axes implies that the spins are not long range ordered and that a major fraction have their orientations distributed in what is described as a hedgehog configuration. As the temperature is raised the Curie law corrected spectral areas decrease markedly as a result of local spin dynamic effects which reduce the transverse relaxation time T_2. The resultant poor signal-to-noise ratio prevents spectra from being recorded above 20 K. The results are consistent with the model proposed in Sec. IV A, which allows for the persistence of dynamical disorder in the K layers at temperatures below 10 K. Further discussion of the spin dynamic effects in terms of the proposed model is given below. It is clear that the relatively sparse interstitial O atoms produce a dramatic change in the electronic properties of the NS material. We consider various physical mechanisms that produce the observed differences between the S and NS NMR spectra.

In order to explain the major changes in the NMR properties that are produced by the nonstoichiometry in $YBaCo_4O_{7.1}$, we focus, in a qualitative way, on changes in the electronic structure produced by the excess oxygen. The continuous distribution of $B_{\rm HF}$ suggests that the Co sites have a variety of local crystal field environments. The hyperfine Hamiltonian has the form $\mathcal{H}_{\rm HF} = \boldsymbol{I} \bullet \boldsymbol{A} \bullet \boldsymbol{S}$ with $\boldsymbol{I}$ the nuclear spin, $\boldsymbol{S}$ the electron spin, and $\boldsymbol{A}$ the hyperfine tensor [16]. If the hyperfine interaction is isotropic the Hamiltonian becomes $\mathcal{H}_{\rm HF} = A\,\boldsymbol{I} \bullet \boldsymbol{S}$ and this form is particularly useful when the contact hyperfine interaction $\mathcal{H}_{\rm C}$ is of dominant importance. For ions in which the orbital angular momentum makes a significant contribution to the hyperfine interaction the Hamiltonian can be written as $\mathcal{H}_{\rm HF} = \mathcal{H}_{\rm C} + \mathcal{H}_{\rm L} + \mathcal{H}_{\rm SD}$, with $\mathcal{H}_{\rm L}$ the orbital contribution and $\mathcal{H}_{\rm SD}$ the spin dipolar part [17,18]. For cases in which the spin-orbit coupling is relatively small compared to the crystal field splitting and second-order perturbation theory applies, the orbital contribution to the hyperfine field at the nucleus is estimated using the relation $B_L = 2\,\mu_B\,\langle r^{-3}\rangle\,\Delta g$, where Δg is the change in the g value produced by spin-orbit coupling, $\langle r^{-3}\rangle$ is the Co ion radial parameter and μ_B the Bohr magneton [19]. The orbital contribution in this limit can be significant, on the order of several tesla, as shown in Mössbauer spectroscopy [19]. The dipolar contribution to the hyperfine field is typically smaller than the contact and orbital contributions and is ignored in the present discussion. The magnetic properties of Co^{2+} and Co^{3+} in T_d symmetry are discussed in Ref. [3] and based on values given there we estimate that for Co^{2+} ($S = 3/2$) the orbital contribution to the magnetic moment is 0.5 μ_B, while for Co^{3+} ($S = 2$) the orbital contribution is 0.2 μ_B. Using these Δg estimates and, as an approximation taking the radial parameters for the two charge and spin states to be similar, we obtain $B_L^{3+}/B_L^{2+} \sim 2.5$. The net field at the nucleus is given by the vector sum of B_C and B_L. The larger orbital contribution for Co^{2+} than for Co^{3+} should be borne in mind in comparing HF NMR resonance frequencies for these two ions in $YBaCo_4O_7$ [15] and other 114 systems. Any buckling of the layers in the NS material, with associated distortions of oxygen tetrahedra from T_d symmetry, or conversion of tetrahedra into octahedra with $O_{\rm h}$ symmetry, will lead to changes in the crystal field for associated Co ions, and consequently changes in the the HF field for these ions. These effects can lead to a distribution of HF fields of the form revealed by the ^{59}Co spectra for $YBaCo_4O_{7.1}$.

In considering the lattice distortions produced by interstitial oxygen in $YBaCo_4O_{7.1}$, it is necessary to allow for two main effects (i) the conversion of a fraction of tetrahedral Co into octahedral Co, as seen in the ordered $YBaCo_4O_8$ phase [10] illustrated in Fig. 1, resulting in changes in the crystal field states as mentioned above, and (ii) oxidation of Co^{2+} ions to smaller Co^{3+} ions and a concomitant modification in bond lengths in the affected oxygen polyhedra. The Co^{2+} to Co^{3+} ratio in $YBaCo_4O_{7.1}$ is 2.3:1, somewhat lower than the 3:1 in

the S material. Our previous work on $YBaCo_4O_7$ has found that the Co^{3+} HF NMR spectral peaks for this system are located at 90, 100, and 120 MHz while the Co^{2+} spectral peaks occur below 70 MHz as shown in Fig. 4 [15]. The conversion of Co^{2+} with NMR spectral features at frequency $f < 70$ MHz into Co^{3+}, which gives peaks at $f > 70$ MHz, is expected to increase the NMR spectral amplitude in the NS crystal in the 90–100 MHz range and to decrease the amplitude of the lower frequency components. While the lineshapes of the two ^{59}Co spectra shown in Fig. 4 are very different, and the amplitudes have not been scaled to allow for variation in the spectrometer sensitivity with frequency, a comparison suggests that the forms are broadly consistent with a change in the Co ion charge state between the S and NS crystals.

C. Cooling rate dependent properties of $YBaCo_4O_{7.1}$

The ZF ^{59}Co spectra obtained following controlled slow cooling (1 K/min) from 290 to 20 K, as shown in Fig. 5, suggest that interstitial oxygen inhomogeneity in the sample is established in this process and that certain local regions give spectra, which are very similar to those obtained for the S material at 20 K. This observation implies some local phase separation linked to a small miscibility gap. For the case of fast cooling (>10 K/min.) from 280 K no NMR signals are observed at 20 K, even following considerable signal averaging. We suggest that the mechanism for the dramatic change in the spectra between the slow-cooling and fast-cooling protocols involves interstitial oxygen clustering that develops in local regions of the crystal during slow cooling but which does not occur in the fast-cooling case. This cooling rate dependent effect requires thermally activated local interstitial oxygen diffusion which results in the nanoscale oxygen inhomogeneity in a slow-cooling experiment. Aging effects involving long-range (~10–100 nm) interstitial oxygen inhomgeneity at 273–300 K have been studied in $YBaCu_3O_{7-\delta}$ (Y123) [20,21]. The aging is accompanied by structural changes from orthorhombic to tetragonal, which occur as a result of the oxygen configuration, without any change of bulk stoichiometry. Long-range oxygen ordering (ordered domain size ~300 nm) has also been reported in $ZrWMoO_8$ at ~200 K [22]. It is likely that similar aging effects occur in $YBaCo_4O_{7.1}$, albeit on a considerably shorter length scale, as long-range ordering that is observed in Y123 has not been detected by x-ray or neutron diffraction in $YBaCo_4O_{7+\delta}$.

D. Comparison of the spin properties of $YBaCo_4O_7$ and $YBaCo_4O_{7.1}$

It is instructive to compare the present results for $YBaCo_4O_{7.1}$ with those for the parent compound $YBaCo_4O_7$, which has a symmetry lowering structural transition from trigonal to orthorhombic at 310 K, and a transition to an AF state, accompanied by a small monoclinic structural distortion, at $T_N = 106$ K. The crystal structure of $YBaCo_4O_{7.1}$ retains trigonal symmetry down to low temperatures and the present results indicate that geometrical frustration prevents long-range ordering in the $\delta = 0.1$ material. The magnetization measurements suggest that freeze-out accompanied by short-range spin ordering of the T spins occurs below $T^* = 80$ K. Based on previous results for the S material [15], it appears likely that a small but significant fraction of the K spins remain dynamic on the NMR time scale (>10 μs) down to $T < 10$ K and may only exhibit frozen behavior well below 4 K. The main features in the temperature dependence of the spin dynamics behavior in $YBaCo_4O_{7.1}$ show some similarity, in broad terms, to that found in $YBaCo_4O_7$ where a large fraction of T spins are AF ordered below $T_N = 106$ K while some of the K spins remain dynamic at temperatures below 10 K [15]. The details of the spin configurations in the S and NS cases are, however, quite different. In $YBaCo_4O_7$, NMR data at $T < 5$ K support a model in which the T spins (more strictly the associated HF fields) are long-range AF ordered along [110] with the K spins in a spin-flop configuration with respect to the T spins [15,23]. Few if any spins make an appreciable angle with the *ab* plane. For $YBaCo_4O_{7.1}$ at 5K in ZF, the majority of the T and K spins are, to a good approximation, isotropically distributed about the *c* axis with a large fraction oriented out of the *ab* plane.

V. CONCLUSION

The NS frustrated antiferromagnet $YBaCo_4O_{7.1}$ has been shown to have exotic spin properties below a transition temperature $T^* = 80$ K. The ground-state spin configuration may be described as a disordered or spin-glass-like system made up of two spin subsystems that exhibit different geometrical frustration behaviors. The magnetization and ZF NMR results are consistent with short-range or intermediate-range ordering of a fraction of the spins at $T < T^*$. Neutron scattering results show broad diffuse scattering peaks at low temperatures consistent with short-range spin correlations [13].

An important driver for the dramatically different magnetic behavior of the NS frustrated AF, compared to the S case, is the persistence to low temperatures of the trigonal lattice symmetry which prevents long-range ordering of spins. In the parent S compound, the symmetry lowering transition at 310 K allows long-range AF spin ordering below $T_N = 106$ K. However, the present findings indicate that the NS material is unlikely to be appropriate as a putative model system in which the structural phase transition has been suppressed to 0 K with dynamical spin correlations persisting to low temperatures. Incorporation of a comparatively small amount of interstitial O in the NS system (1.4%) leads to major changes in the physical properties compared to those of the S material.

Based, in part, on the results for the S material [15], it appears likely that the T spins form a locally ordered component below 80 K. In contrast, a fraction of the spins that, we suggest, are in the K layers, remain dynamically disordered at lower temperatures with a significant fraction still dynamic below 10 K. In addition, evidence has been obtained for local interstitial oxygen inhomogeneity in slow cooling experiments from 280 to 20 K.

ACKNOWLEDGMENTS

The work was supported by the NSF under Cooperative Agreement No. DMR-0654118 and by the State of Florida. J.S.B. acknowledges funding from NSF-DMR 1005293. Support from the US DOE, Office of Science, Office of

Basic Energy Sciences, Division of Materials Science and Engineering provided to J.F.M. and H.Z. at Argonne under contract number DE-AC02-06CH211357 and to T.B. and T.S. at the NHMFL under contract number DE-SC0008832 is acknowledged. The ac susceptibility measurements were made on PPMS instruments in the Center for Applied Superconductivity and in the Department of Chemistry at Florida State University.

[1] L. C. Chapon, P. G. Radaelli, H. Zheng, and J. F. Mitchell, Phys. Rev. B **74**, 172401 (2006).
[2] P. Manuel, L. C. Chapon, P. G. Radaelli, H. Zheng, and J. F. Mitchell, Phys. Rev. Lett. **103**, 037202 (2009).
[3] N. Hollmann, Z. Hu, M. Valldor, A. Maignan, A. Tanaka, H. H. Hsieh, H.-J. Lin, C. T. Chen, and L. H. Tjeng, Phys. Rev. B **80**, 085111 (2009).
[4] D. D. Khalyavin, P. Manuel, J. F. Mitchell, and L. C. Chapon, Phys. Rev. B **82**, 094401 (2010).
[5] D. D. Khalyavin, P. Manuel, B. Ouladdiaf, A. Huq, P. W. Stephens, H. Zheng, J. F. Mitchell, and L. C. Chapon, Phys. Rev. B **83**, 094412 (2011).
[6] M. Karpinnen, H. Yamauchi, S. Otani, T. Fujita, T. Motohashi, Y.-H. Huang, M. Valkeapää, and H. Fjellvåg, Chem. Mater. **18**, 490 (2006).
[7] S. Räsänen, H. Yamauchi, and M. Karppinnen, Chem. Lett. **37**, 638 (2008).
[8] H. Hao, L. Zhao, J. Hu, X. Hu, and H. Hou, J. Rare Earths **27**, 815 (2009).
[9] Y. Jia, H. Jiang, M. Valkeapää, H. Yamauchi, M. Karppinnen, and E. I Kauppinen, J. Am. Chem. Soc. **131**, 4880 (2009).
[10] O. Chmaissem, H. Zheng, A. Huq, P. W. Stephens, and J. F. Mitchell, J. Solid State Chem. **181**, 664 (2008).
[11] E. V. Tsipis, J. C. Waerenborgh, M. Avdeev, and V. V. Kharton, J. Solid State Chem. **182**, 640 (2009).
[12] J. L. Izquierdo, J. F. Montoya, A. Gómez, O. Arnache, T. Wolf, and O. Morán, Solid State Comm. **150**, 1951 (2010).
[13] S. Avci, O. Chmaissem, H. Zheng, A. Huq, P. Manuel, and J. F. Mitchell, Chem. Mater. **25**, 4188 (2014).
[14] A. Huq, J. F. Mitchell, H. Zheng, L. C. Chapon, P. G. Radaelli, K. S. Knight, and P. W. Stephens, J. Solid State Chem. **179**, 1136 (2006).
[15] M. J. R. Hoch, P. L. Kuhns, S. Yuan, T. Besara, J. B. Whalen, T. Siegrist, A. P. Reyes, J. S. Brooks, H. Zheng, and J. F. Mitchell, Phys. Rev. B **87**, 064419 (2013).
[16] C. P. Slichter, *Principles of Magnetic Resonance*, 3rd ed. (Springer-Verlag, Heidelberg, 1996).
[17] R. E. Watson and A. J. Freeman, Phys. Rev. **120**, 1134 (1960).
[18] R. E. Watson and A. J. Freeman, Phys. Rev. **123**, 2027 (1961).
[19] P. Gütlich, K. M. Hasselbach, H. Rummel, and H. Spiering, J. Chem. Phys. **81**, 1396 (1984).
[20] B. W. Veal, A. P. Paulikas, Hoydoo You, Hao Shi, Y. Fang, and J. W. Downey, Phys. Rev. B **42**, 6305 (1990).
[21] B. W. Veal, H. You, A. P. Paulikas, H. Shi, Y. Fang, and J. W. Downey, Phys. Rev. B **42**, 4770 (1990).
[22] S. Allen and J. S. O. Evans, J. Mater. Chem. **14**, 151 (2004).
[23] There is a controversy surrounding the somewhat different low-temperature spin configurations for the kagome layers in $YBaCo_4O_7$ obtained, firstly, from neutron diffraction as given in Ref. [[5]], and, secondly, from NMR spectra as given in Ref. [[15]]. The NMR results are based on the HF field orientations, which are assumed to be close to antiparallel to the spin orientations.